Published in final edited form as:
Radiat Res. 2012 October ; 178(4): 321–327.

A Gated-7T MRI Technique for Tracking Lung Tumor Development and Progression in Mice after Exposure to Low Doses of Ionizing Radiation

John D. Olson[a], **Matthew C. Walb**[b,c], **Joseph E. Moore**[d], **Albert Attia**[b], **Heather L. Sawyer**[a], **Jennifer E. McBride**[d], **Kenneth T. Wheeler**[e,f,g], **Mark Steven Miller**[d,f,g], and **Michael T. Munley**[b,f,g,1]

[a]Center for Biomolecular Imaging, Wake Forest School of Medicine, Winston-Salem, North Carolina

[b]Department of Radiation Oncology, Wake Forest School of Medicine, Winston-Salem, North Carolina

[c]Department of Physics, Wake Forest School of Medicine, Winston-Salem, North Carolina

[d]Department of Cancer Biology, Wake Forest School of Medicine, Winston-Salem, North Carolina

[e]Department of Radiology, Wake Forest School of Medicine, Winston-Salem, North Carolina

[f]Department of Thoracic Oncology Center of Excellence, Wake Forest School of Medicine, Winston-Salem, North Carolina

[g]Comprehensive Cancer Center, Wake Forest School of Medicine, Winston-Salem, North Carolina

[c]Wake Forest University, Winston-Salem, North Carolina

Abstract

A gated-7T magnetic resonance imaging (MRI) application is described that can accurately and efficiently measure the size of in vivo mouse lung tumors from ~0.1 mm^3 to >4 mm^3. This MRI approach fills a void in radiation research because the technique can be used to noninvasively measure the growth rate of lung tumors in large numbers of mice that have been irradiated with low doses (<50 mGy) without the additional radiation exposure associated with planar X ray, CT or PET imaging. High quality, high resolution, reproducible images of the mouse thorax were obtained in ~20 min using: (1) a Bruker 7T micro-MRI scanner equipped with a 60 mm inner diameter gradient insert capable of generating a maximum gradient of 1000 mT/m; (2) a 35 mm inner diameter quadrature radiofrequency volume coil; and (3) an electrocardiogram and respiratory gated Fast Low Angle Shot (FLASH) pulse sequence. The images had an in-plane image resolution of 98 μm and a 0.5 mm slice thickness. Tumor diameter measured by MRI was highly correlated (R^2 = 0.97) with the tumor diameter measured by electronic calipers. Data generated with an initiation/promotion mouse model of lung carcinogenesis and this MRI technique demonstrated that mice exposed to 4 weekly fractions of 10, 30 or 50 mGy of CT radiation had the same lung tumor growth rate as that measured in sham-irradiated mice. In summary, this high-field, double-gated MRI approach is an efficient way of quantitatively tracking lung tumor development and progression after exposure to low doses of ionizing radiation.

[1]Address for correspondence: Department of Radiation Oncology, Wake Forest School of Medicine, Medical Center Blvd., Winston-Salem, NC 27157; mmunley@wakehealth.edu.

INTRODUCTION

Lung cancer is responsible for more deaths than any other form of cancer (1, 2). This provides a strong impetus to study lung cancer induction and progression. Noninvasive imaging, including planar X-ray techniques, X-ray computed tomography (CT), and positron emission tomography (PET) are routinely used to diagnose and stage lung cancer, and to plan and evaluate the efficacy of lung cancer treatments (3–9). However, all of these imaging techniques involve exposure to ionizing radiation, which confounds the interpretation of small animal preclinical studies on low-dose radiation-induced carcinogenesis and normal tissue late effects. Ultrasound (10, 11) and magnetic resonance imaging (MRI) (12) are two nonionizing techniques that have the potential to solve this problem. However, the utility of ultrasound is limited at this time because it can only reliably detect tumors located at the lung and chest wall interface. In contrast, MRI combined with 3-dimensional image analysis has the potential to obtain quantitative information on tumor number and size throughout the entire lung. Thus, the development of a high throughput MRI technique that can serially collect quantitative information on lung tumor induction and progression, after exposing small animals to mGy doses of ionizing radiation, has the potential to make a major contribution to our understanding of low-dose radiation effects in the lung.

Mice are frequently used for preclinical cancer research studies because they reproduce efficiently, grow quickly and can be genetically modified. Transgenic mice have been generated that allow one to design experiments that test specific hypotheses about pathways and gene involvement in lung tumor development and their response to treatment (13, 14). Mouse lung tumors have been successfully imaged *in vivo* using high-field MRI (15–24). However, there is only one report where an MRI technique has been used to serially track lung tumor development and response to treatment in mice. In that study, the starting size for growth curves was limited to tumors with diameters ≥1 mm and a volume of ~0.5 mm^3 (20).

The 7T MRI Lab in the Center for Biomolecular Imaging at the Wake Forest School of Medicine recently acquired a high-power gradient coil insert specifically for imaging mice. This new gradient coil was used initially to routinely perform electrocardiogram (ECG)- and respiratory-gated cardiac and atherosclerosis imaging in mice. However, examination of the cardiac MRI images suggested that a similar imaging protocol might provide the high spatial resolution required to identify and quantitatively track the size of *in vivo* murine lung tumors over a prolonged period of time. The best published *in vivo* MRI technique for measuring lung tumors had a 0.55 mm slice thickness and a 155 μm in-plane spatial resolution that measured *in vivo* mouse lung tumors with a minimum diameter of ~0.5 mm and an estimated volume of ≥0.3 mm^3 in ~20 min. *In vivo* growth rates were determined over <1 tumor volume doubling time (20). Thus, the goal of this study was to present an MRI technique with a resolution that could accurately measure *in vivo* mouse lung tumors with a diameter <0.5 mm and a volume ≤0.3 mm^3 in ~20 min so that *in vivo* lung tumor growth rates could be generated over ≥2 volume doubling times after exposure to low doses (≤50 mGy) of ionizing radiation. To accomplish this goal, we selected 3 mouse models of lung cancer development in current and former smokers (25–28) that are presently being used to evaluate the carcinogenic risk from low-dose CT exposures where an accurate estimate of the growth rate is important for interpretation of the data (29).

MATERIALS AND METHODS

Mouse Models and Treatment Protocols

All procedures in this study were approved by our Institutional Animal Care and Use Committee. A bitransgenic mouse that conditionally expresses a mutant human Ki-*ras*^{G12C} gene in a doxycycline (DOX) inducible and lung-specific manner, and a complete lung carcinogenesis model were used to compare the size of lung tumors measured *in vivo* by the MRI technique with the size measured by electronic calipers after excision of the lungs. The bitransgenic mouse model represents the earliest stages of lung cancer development where hyperplastic foci and very small, benign adenomas are measurable 3–9 months after initiation of the DOX treatment (25). The complete carcinogenesis mouse model uses a tobacco-specific carcinogen to induce lung tumors that recapitulate all stages of lung adenocarcinoma development (26).

For experiments with the bitransgenic model, 8-week-old mice were continuously administered 500 μg/mL of DOX in their drinking water. One week after initiating the DOX treatment, groups of mice were either sham-irradiated or whole-body irradiated with 5, 15 or 25 mGy/week for 4 weeks using our clinical CT scanner. For experiments with the complete carcinogenesis model, 8-week-old AJ mice were injected i.p. with 100 mg/kg of the nicotine-derived nitrosamine ketone, 4-*N*-methyl-*N*-nitrosomino-1-(3-pyridyl)-1-butanone (NNK), dissolved in phosphate-buffered saline (5 mg/ml; 0.5 ml per 25 gm mouse). One week later, the NNK mice were either sham-irradiated or whole-body irradiated with 10, 30 or 50 mGy/week for 4 weeks using our clinical CT scanner. At 9 months after the last radiation fraction, the largest diameter of several tumors identified by MRI in both the bitransgenic and NNK mice was measured *in vivo* using our MRI technique and *ex vivo* using electronic calipers.

An initiation/promotion lung carcinogenesis mouse model that used 3-methylcholanthrene (MC) as the initiating agent and butylated hydroxytoluene (BHT) as the promoter (27) was employed to generate *in vivo* lung tumor growth curves for mice that were either sham-irradiated or irradiated with low doses of CT radiation. Eight-week-old Balb/c mice were injected i.p. with 15 mg/kg of the genotoxic chemical carcinogen, MC, dissolved in corn oil (0.75 mg/ml; 0.5 ml per 25 gm mouse). Starting 1 week later, 150 mg/kg of BHT dissolved in corn oil (7.5 mg/ml; 0.5 ml per 25 gm mouse) was injected i.p. each week for 6 weeks to provide a promotional stimulus. This mouse model also recapitulates all stages of lung adenocarcinoma development in current and former smokers (28). Starting the week of the third BHT injection, mice were either sham-irradiated or whole-body irradiated with 10, 30 or 50 mGy/week for 4 weeks using our clinical CT scanner. At 3 months after the last radiation fraction, tumors with a minimum diameter of ~0.2 mm were identified and their tumor volume was determined using our MRI technique. These identical tumors were remeasured by MRI at 6 and 9 months after irradiation, and growth curves were constructed from the tumor volume measurements.

7T MRI Procedure

MR imaging experiments were performed using a Bruker Biospec 70/30 7.0 Tesla horizontal bore microMR scanner (Bruker Biospin, Billerica, MA). The magnet was fitted with a 60 mm inner diameter (I.D.) BGA-6S gradient insert (Bruker Biospin) capable of generating a maximum magnetic field gradient of 1,000 mT/m. A 35 mm I.D. quadrature volume radiofrequency (RF) coil tuned to 300.2 MHz was used for MR signal transmission and reception.

Mice were anesthetized (~2 min) initially in a chamber using a mixture of oxygen (3 L/min) and isofluorane (3%). Once an animal was fully anesthetized, optical lubricant was placed

on each eye to prevent drying. The mouse was then moved to the MRI magnet room and placed in a supine position on a plastic bed fitted with a nose cone that continuously supplied oxygen (1.0 L/min) and isofluorane (1.5%) during the scan. Neonatal ECG leads (3M, St. Paul, MN) were attached to the front paws to monitor the heart rate for cardiac gating. A respiration pillow (SAII Instruments, Stony Brook, NY) was taped over the mouse's abdomen to monitor the breathing rate for respiratory gating. A temperature probe was placed under the mouse to monitor the skin temperature. The mouse was heated to a skin temperature of 32°C to maintain a core temperature of approximately 37°C by blowing thermostatically controlled warm air into the magnet's bore. The anesthesia was adjusted to maintain a constant breathing rate so that there is little variability in MR characteristics, imaging time, and imaging quality during and between runs. The ECG leads, respiration pillow and temperature probe were all connected with interface modules to a computer that ran the PC-SAM small animal monitoring and gating software (SAII Instruments). The plastic bed was placed in the RF coil so that the mouse's thoracic cavity was positioned both in the center of the homogeneous RF field and at the isocenter of the magnet. Each channel of the quadrature coil was tuned and matched to 300.2 MHz. Total set-up time was ~4 min.

A 3-plane localizer scout scan (~1 min) was acquired using an ungated Rapid Acquisition with Relaxation Enhancement (RARE) pulse sequence with the following parameters: repetition time (TR) = 1,500 ms, echo time (TE) =30 ms, field of view (FOV) =4 cm, matrix =128 ×128, slice thickness =2 mm and number of excitations (NEX) = 1. This scan verified that the mouse's thoracic cavity was at the isocenter of the magnet and RF coil. If not, the mouse's position was adjusted, and a new 3-plane scout scan (~1 min) was acquired. When the mouse was properly positioned, low-resolution coronal and axial scout scans (~2 min) were acquired to allow precise positioning and orientation of the high-resolution scan. A gated Fast Imaging with Steady State Precession (FISP) pulse sequence was used for the coronal and axial scout scans. Parameters for the FISP scans were: TR = 2.8 ms, TE = 1.4 ms, Flip Angle (FA) = 30 degrees, FOV = 4 cm, matrix = 128 × 128, slice thickness = 2 mm, NEX = 1.

Coronal slice planes of the high-resolution scan were positioned using the axial and coronal FISP scout scans. The axial FISP images allowed the high-resolution coronal slices to be oriented so that they were parallel to a line that was tangent to the back of the lungs. The coronal FISP images allowed the high-resolution coronal slices to be positioned so that the most rostral and caudal portions of the lungs were included in the scan. The high-resolution scan (~12 min) was acquired using a Fast Low Angle Shot (FLASH) pulse sequence gated so that acquisition was triggered on the ECG R-waves that did not occur during breathing. The FLASH sequence parameters were: TR = 215 ms, TE =2.2 ms, FA =30 degrees, FOV =2.5 cm, matrix =256 × 256, in-plane spatial resolution =98 μm, slice thickness =0.5 mm, and NEX = 4.

When the high-resolution scan was completed, all monitoring electrodes and probes were disconnected, and the mouse was removed from the 7T scanner and placed on a warming pad (~1 min) to recover before being returned to its cage.

Image Analysis

The resulting 7T MR images were quantitatively analyzed using the TeraRecon (Foster City, CA) and MIPAV (Medical Image Processing, Analysis and Visualization, http://mipav.cit.nih.gov/) image analysis packages (Fig. 1). These image analysis systems allow for tumor identification, localization, and measurement in 3 dimensions (3D). To determine the tumor volume, each tumor identified in a 0.5 mm slice was manually contoured (Fig. 2), and the computer program determined the volume occupied by the tumor from the area of pixels within each contour multiplied by the slice thickness. If the tumor was contoured in 2

or more slices, the tumor volume was determined in each slice as described above, and the total tumor volume was determined by summing the volumes from each slice. This method allowed one to more accurately measure the volume of irregularly shaped tumors (Fig. 2).

Data Analysis

The diameters of lung tumors in bitransgenic and NNK mice measured *in vivo* by MRI were plotted as a function of the diameter measured *ex vivo* using electronic calipers. These data were subjected to a least squares linear regression analysis to determine if a 1:1 relationship existed between the 2 measurements. *In vivo* tumor volume doubling times were determined for the sham-irradiated and irradiated groups of MC + BHT mice using a regression analysis of the $\log_e$ transform of the tumor volumes determined by MRI as a function of the postirradiation time.

RESULTS

Our double-gated FLASH sequence with coronal slice plane orientation was capable of producing MRI images with a 98 μm in-plane resolution and a slice thickness of 0.5 mm in ~20 min/mouse. The 98 μm in-plane spatial resolution represented a 37% improvement over the best previously published *in vivo* murine lung tumor MRI resolution of 155 μm (20). The resulting voxel size was ~0.0048 mm^3 compared to the previous best voxel size of ~0.013 mm^3. Thus, our MRI technique has ~2.7 times as many voxels/unit volume as does the previous best MRI technique. This allowed us to identify, track and quantify lung tumors that are ≤0.5 mm in diameter and that are in close proximity to one another. Depending on the location, shape and density, tumors as small as ~0.2 mm in diameter (Fig. 3) or having a volume of ~0.1 mm^3 can be identified, tracked and quantitatively measured (Fig. 3, Table 1). However, diffuse tumors with a diameter of <0.3 mm at 3 months postirradiation frequently require the images obtained at 6 and 9 months to locate and estimate the tumor volume.

When the diameters of individual lung tumors determined *in vivo* with the MRI technique were compared to the diameters of the same tumors measured *ex vivo* after excising the lungs, the data were fitted to a line that was statistically identical to y = x with a correlation coefficient (R^2) of 0.97 independent of tumor model and growth rate (Fig. 4).

Using our MRI technique, the average growth rates of lung tumors were determined in sham-irradiated MC + BHT mice or MC + BHT mice subjected to 4 weekly fractions of 10, 30 or 50 mGy doses of whole-body CT radiation. The average tumor volume for these groups ranged from <0.2 mm^3 to >4.0 mm^3 over a 3–9 month postirradiation period (Table 1). The variability of the individual tumor volume measurements is reported in Table 1 as standard errors that were typically 20–30% of the corresponding means. The average tumor volume doubling times ranged from 1.5–1.8 months with correlation coefficients of 0.84–0.97. These doubling times were not statistically different ($P > 0.05$) between the sham-irradiated and irradiated mice. The growth rate variability obtained from a regression analysis of the tumor volume data ranged from 9–18% of the tumor volume doubling time, and the range of growth rates for individual tumors was as large as a factor of 2. However, a range of this magnitude often includes potential outliers. If an outlier exclusion test such as Chauvenet's criterion (30) was applied to the data, only 2 of the 50 tumors that were evaluable could be excluded. Because exclusion of these 2 tumors did not change the interpretation of these data, they were included in the analyses shown in Table 1. These data indicated that small fractionated doses of CT radiation do not affect the *in vivo* tumor growth rate in this initiation/promotion lung carcinogenesis model.

DISCUSSION

We have been studying the carcinogenic effects of low-dose CT scans using mouse models of current and former smokers (29). Any radiation-induced tumors in these experiments could be due to either initiation or promotion mechanisms. Distinguishing between these mechanisms requires information on the *in vivo* growth rate and the final size of the tumors in irradiated and unirradiated mice. The final tumor size can be estimated efficiently by euthanizing the mice, excising the lungs, and measuring the tumor size with electronic calipers at the end of the experiment. However, the *in vivo* growth rate must be estimated either by: (1) euthanizing irradiated and unirradiated mice at various times and measuring the tumor size in their excised lungs, or (2) a noninvasive imaging technique. The former method requires many mice and provides information only on the population growth rate. The latter method requires only relatively few mice and provides information on both the population and individual tumor growth rates. Thus, a noninvasive method for measuring the size of lung tumors *in vivo* is critical for determining both the population and individual tumor growth rates in low-dose carcinogenesis studies.

A cost-effective, noninvasive method for measuring the size of mouse lung tumors must have a high throughput. CT has the highest throughput of all noninvasive imaging techniques that have 3D reconstruction capability for measuring the volumes of irregularly shaped tumors. However, the total CT imaging lung dose required to construct an *in vivo* tumor volume growth curve greatly exceeds the experimental dose in low-dose (≤50 mGy) carcinogenesis studies, thereby confounding interpretation of the low-dose data (29). MRI is the most promising of all noninvasive imaging techniques that do not use ionizing radiation and have 3D reconstruction capability for tumor volume measurements. The limitations of MRI for these studies involve the in-plane resolution, slice thickness, image quality, imaging time, and 3D reconstruction/quantification software.

In this study, we demonstrated a cardiac and respiratory-gated 7T MRI protocol to minimize these limitations and to track *in vivo* lung tumor growth in lung carcinogenesis mouse models after exposure to fractionated doses of CT radiation ≤50 mGy. To accomplish this, 3 pulse sequences were tested: (1) a Rapid Acquisition with Relaxation Enhancement (RARE) pulse sequence with echo trains of 8 and 4 echoes, (2) a Fast Imaging with Steady State Precession (FISP) sequence, and (3) a Fast Low Angle Shot (FLASH) pulse sequence. We started with these three sequences because they were already in use by our 7T Lab for murine cardiac imaging. The RARE sequence yielded high-resolution images that could be used to measure tumors. However, it had long acquisition times (~30 min) that made it impractical for projects that required a large number of scans. The FISP (~8 min) and FLASH (~12 min) sequences were significantly faster than the RARE sequence. Ultimately, the FLASH sequence was selected over the quicker FISP sequence because FISP susceptibility artifacts decreased the ability to distinguish tumor from the surrounding normal tissue (31, 32).

Most of the published MRI techniques for imaging mouse lung tumors acquire images with an axial slice plane orientation (21–24). For a mouse lying in a supine position and image slices of the same thickness, the axial slice plane orientation requires the greatest number of slices (~60) to cover the entire lung cavity. We selected a coronal slice orientation to cover the entire lung cavity with the fewest number of slices (~30) to substantially reduce the acquisition time. The selection of coronal slice plane orientation to reduce acquisition time is not unprecedented. Schuster *et al.* (18), Garbow *et al.* (19), and Degrassi *et al.* (20) all acquired MR images of mouse lung tumors using coronal slices to reduce the total slice number and acquisition time. However, their in-plane resolution and slice thickness limited their ability to quantitatively measure tumors to those with a diameter of ~0.5 mm and a

volume of ~0.5 mm^3. Our protocol can quantitatively measure lung tumors with a diameter of ~0.2 mm and a volume of ~0.1 mm^3 (Fig. 1, Table 1). This is important because lung tumors in most mouse models grow rapidly, producing a tumor burden that requires euthanizing the mice in a short time period. For example, starting with lung tumors that had a diameter of ~1 mm and a volume of ~0.5 mm^3, Degrassi *et al.* (20) only followed tumor growth for <1 volume doubling time over <50 days after treatment. With our protocol, we quantitatively followed slow growing lung tumors for >3 volume doubling times over 9 months postirradiation (Table 1).

Our 7T MRI protocol is also cost effective. With two people working, it is possible to scan 12 mice in 4 h (3 mice/h). As one person takes a mouse from the scanner and removes the ECG leads and the respiration pillow, the second person begins anesthetizing the next animal. Overlapping the end of the previous mouse's scan with the beginning of the next mouse's scan prevents the total prep and scan time from exceeding 20 min/mouse. If we were to sacrifice mice at each of the times to generate growth curves, we would need at least 2 times as many mice at a cost that would be far greater, especially for studies with transgenic mice.

Finally, the TeraRecon and MIPAV image analysis software described in the Image Analysis section permits one to estimate the volumes of irregularly shaped tumors more accurately than can be obtained by measuring 2 diameters in MRI, CT or PET images and calculating the tumor volume by assuming a spherical or ellipsoidal shape. Rarely do the tumors in our 3 lung carcinogenesis models have a shape that approximates a true sphere or an ellipsoid (Figs. 1–3). It is indeed more difficult to get an accurate estimation of lung tumor volumes from measurements with electronic calipers. Of necessity, these measurements are restricted to tumors near the lung surface and usually only 2 dimensions can be obtained. The difference between the contoured MRI volume and that calculated using an equation often employed by cancer biologists to obtain tumor volume or the equation for an ellipsoid can be as large as 40% (Fig. 2). In general, we found that tumors tended to be nonspherical at 9 months postirradiation. Thus, the examples in Fig. 2 are both illustrative and representative of tumor shape for this model.

In summary, a double-gated 7T MRI technique is described that is capable of generating high-quality lung images with an in-plane resolution of 98 μm and a slice thickness of 0.5 mm in ~20 min/mouse. This technique, along with the analysis software, permits the identification, tracking, and quantification of lung tumors *in vivo* with a diameter of ~0.2 mm and a volume of ~0.1 mm^3, approximately an 80% reduction in tumor size over the best previously published technique (20). Using this technique, we were able to measure accurately (R^2 = 0.84–0.97) *in vivo* lung tumor growth rates over >3 tumor volume doubling times and 9 months after irradiation with mGy doses of ionizing radiation (Table 1). Consequently, this high-field double-gated MRI technique appears to be an efficient way of quantitatively tracking lung tumor development and progression after exposure to low doses of ionizing radiation.

Acknowledgments

This study was supported by a National Cancer Institute grant, R01-CA136910 (MTM), a Wake Forest University Cancer Center Support Grant, P30-CA12197 and the Wake Forest Thoracic Oncology Center of Excellence. The authors thank Michael E. Robbins, Ph.D., for his critical review of this manuscript.

References

1. Division of Cancer Prevention and Control, National Center for Chronic Disease Prevention and Health Promotion. Centers for Disease Control and Prevention. (http://www.cdc.gov/cancer/lung/statistics/index.htm) [Page last updated: November 23, 2010, cited: September 7, 2011]
2. Jemal A, Siegel R, Xu J, Ward E. Cancer statistics, 2010. Cancer J Clin. 2010; 60:277–300.
3. National Lung Screening Trial Research Team. The national lung cancer screening trial: overview and study design. Radiology. 2011; 258:243–53. [PubMed: 21045183]
4. Pawaroo D, Cummings NM, Musonda P, Rintoul RC, Rassl D, Beadsmoore C. Non-small cell lung carcinoma: accuracy of PET/CT in determining the size of T1 and T2 primary tumors. AJR Am J Roentgenol. 2011; 196:1176–81. [PubMed: 21512089]
5. Fischer B, Lassen U, Mortensen J, Larsen S, Loft A, Bertelsen A, et al. Preoperative staging of lung cancer with combined PET-CT. N Engl J Med. 2009; 361(1):32–9. [PubMed: 19571281]
6. Hocking WG, Hu P, Oken MM, Winslow SD, Kvale PA, Prorok PC, et al. Lung cancer screening in the randomized Prostate, Lung, Colorectal, and Ovarian (PLCO) Cancer Screening Trial. J Natl Cancer Inst. 2010; 102:722–31. [PubMed: 20442215]
7. Mohammed TL, White CS, Pugatch RD. The imaging manifestations of lung cancer. Semin Roentgenol. 2005; 40:98–108. [PubMed: 15898408]
8. Pinilla I, Rodriguez-Vigil B, Gomez-Leon N. Integrated FDG PET/CT: utility and applications in clinical oncology. Clin Med Oncol. 2:181–98. [PubMed: 21892279]
9. Munley MT, Marks LB, Scarfone C, Sibley GS, Patz EF Jr, Turkington TG, et al. Multimodality nuclear medicine imaging in three-dimensional radiation treatment planning for lung cancer: challenges and prospects. Lung Cancer. 1999; 23:105–14. [PubMed: 10217614]
10. Zhou YQ, Foster FS, Nieman BJ, Davidson L, Chen XJ, Henkelman RM. Comprehensive transthoracic cardiac imaging in mice using ultrasound biomicroscopy with anatomical confirmation by magnetic resonance imaging. Physiol Genomics. 2004; 18:232–44. [PubMed: 15114000]
11. Herth FJ. Nonsurgical staging of the mediastinum: EBUS and EUS. Semin Respir Crit Care Med. 2011; 32:62–8. [PubMed: 21500125]
12. Hochhegger B, Marchiori E, Sedlaczek O, Irion K, Heussel CP, Ley S, et al. MRI in lung cancer: a pictorial essay. Br J Radiol. 2011; 84:661–8. [PubMed: 21697415]
13. Dutt A, Wong KK. Mouse models of lung cancer. Clin Cancer Res. 2006; 12:4396s–402s. [PubMed: 16857817]
14. Shaw AT, Kirsch DG, Jacks T. Future of early detection of lung cancer: the role of mouse models. Clin Cancer Res. 2005; 11:4999s–5003s. [PubMed: 16000603]
15. Asanuma T, Ohkura K, Yamamoto T, Kon Y, Shimokawa S, Kuwabara M. Three-dimensional magnetic resonance imaging of lung and liver tumors in mice by use of transversal multislice magnetic resonance images. Comp Med. 2001; 51:138–44. [PubMed: 11922177]
16. Xu S, Gade TP, Matei C, Zakian K, Alfieri AA, Hu X, et al. In vivo multiple-mouse imaging at 1.5 T. Magn Reson Med. 2003; 49:551–7. [PubMed: 12594759]
17. Garbow JR, Zhang Z, You M. Detection of primary lung tumors in rodents by magnetic resonance imaging. Cancer Res. 2004; 64:2740–2. [PubMed: 15087388]
18. Schuster DP, Kovacs A, Garbow J, Piwnica-Worms D. Recent advances in imaging the lungs of intact small animals. Am J Respir Cell Mol Biol. 2004; 30:129–38. [PubMed: 14729505]
19. Garbow JR, Wang M, Wang Y, Lubet RA, You M. Quantitative monitoring of adenocarcinoma development in rodents by magnetic resonance imaging. Clin Cancer Res. 2008; 14:1363–7. [PubMed: 18316556]
20. Degrassi A, Russo M, Nanni C, Patton V, Alzani R, Giusti AM, et al. Efficacy of PHA-848125, a cyclin-dependent kinase inhibitor, on the K-Ras(G12D)LA2 lung adenocarcinoma transgenic mouse model: evaluation by multimodality imaging. Mol Cancer Ther. 2010; 9:673–81. [PubMed: 20197397]
21. Roa WH, Azarmi S, Al-Hallak MH, Finlay WH, Magliocco AM, Lobenberg R. Inhalable nanoparticles, a non-invasive approach to treat lung cancer in a mouse model. J Contr Rel. 2011; 150:49–55.

22. Singh SP, Han L, Murali R, Solis L, Roth J, Ji L, et al. SSTR2-based reporters for assessing gene transfer into non-small cell lung cancer: evaluation using an intrathoracic mouse model. Hum Gene Ther. 2011; 22:55–64. [PubMed: 20653396]
23. Engelman JA, Chen L, Tan X, Crosby K, Guimaraes AR, Upadhyay R, et al. Effective use of PI3K and MEK inhibitors to treat mutant Kras G12D and PIK3CA H1047R murine lung cancers. Nat Med. 2008; 14:1351–6. [PubMed: 19029981]
24. Zhou X, Bao H, Al-Hashem R, Ji H, Albert M, Wong KK, et al. Magnetic resonance imaging of the response of a mouse model of non-small cell lung cancer to tyrosine kinase inhibitor treatment. Comp Med. 2008; 58:276–81. [PubMed: 18589870]
25. Floyd HS, Farnsworth CL, Kock ND, Mizesko MC, Little JL, Dance ST, et al. Conditional expression of the mutant Ki-*ras*^{G12C} allele results in formation of benign lung adenomas: Development of a novel mouse lung tumor model. Carcinogenesis. 2005; 26:2196–206. [PubMed: 16051643]
26. Devereux TR, Belinsky SA, Maronpot RR, White CM, Hegi ME, Patel AC, et al. Comparison of pulmonary O6-methylguanine DNA adduct levels and Ki-ras activation in lung tumors from resistant and susceptible mouse strains. Molec Carcinog. 1993; 8:177–85. [PubMed: 8216736]
27. Malkinson AM, Koski KM, Evans WA, Festing MF. Butylated hydroxytoluene exposure is necessary to induce lung tumors in BALB mice treated with 3-methylcholanthrene. Cancer Res. 1997; 57:2832–4. [PubMed: 9230183]
28. Malkinson AM. Primary lung tumors in mice: an experimentally manipulable model of human adenocarcinoma. Cancer Res. 1992; 52(9 Suppl):2670s–6s. [PubMed: 1562998]
29. Munley MT, Moore JE, Walb MC, Isom SP, Olson JD, Zora JG, et al. Cancer prone mice expressing the Ki-*ras*^{G12C} gene show increased lung carcinogenesis following CT screening exposures. Radiat Res. 2011; 176:842–8. [PubMed: 21962004]
30. Barnett, V.; Lewis, T. Outliers in statistical data. 3. Chichester: J. Wiley and Sons; 1994.
31. Martirosian P, Boss A, Fenchel M, Deimling M, Schäfer J, Claussen CD, et al. Quantitative lung perfusion mapping at 0.2 T using FAIR True-FISP. MRI Magn Reson Med. 2006; 55:1065–74.
32. Schäfer JF, Vollmar J, Schick F, Seemann MD, Mehnert F, Vonthein R, et al. Imaging diagnosis of solitary pulmonary nodules on an open low-field MRI system-comparison of two MR sequences with spiral CT. Rofo. 2002; 174:1107–14. [PubMed: 12221568]

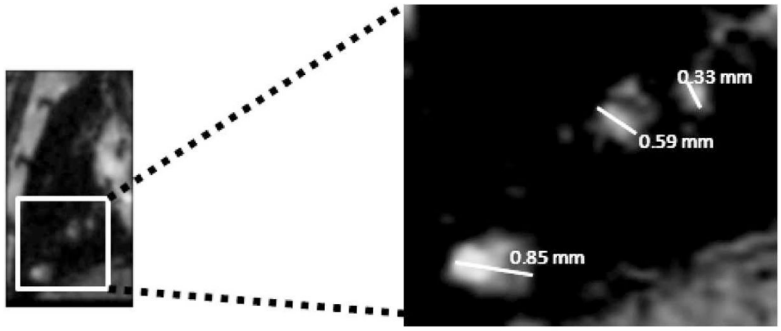

FIG. 1.

A representative double-gated 7T MRI image of a bitransgenic mouse thorax illustrating our sub-millimeter spatial resolution. Although the smallest tumor in this image has a measured diameter of 0.33 mm, compact tumors with a diameter of ~0.2 mm could be identified, tracked, and their volume determined over the period from 3–9 months postirradiation.

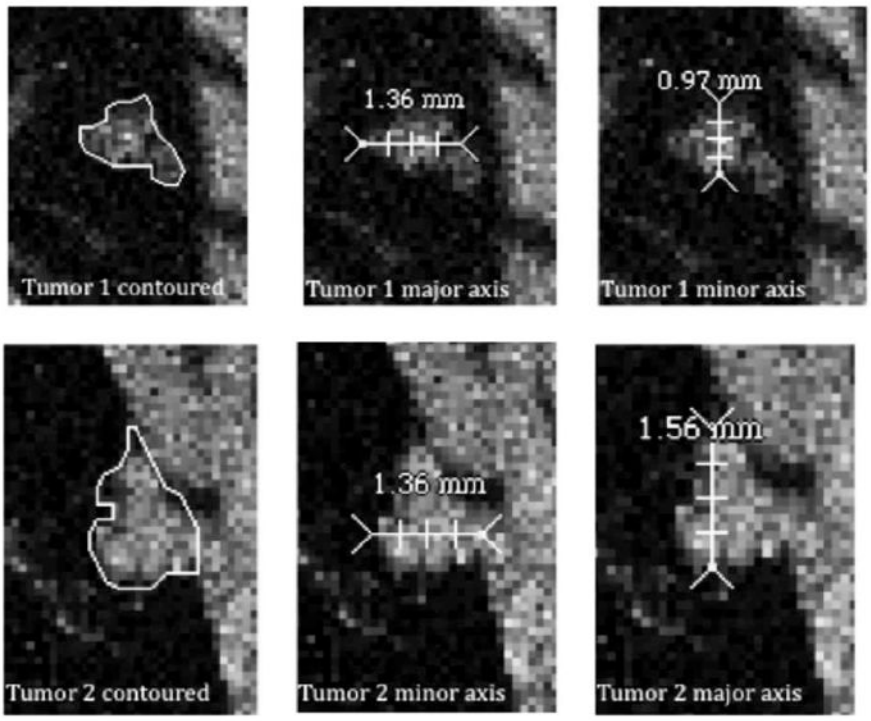

FIG. 2.

Contoured tumors from an MC+BHT mouse 9 months after 4 fractions of 30 mGy. Tumor volume was measured from the MR images or was calculated from the major and minor diameters using the equation $0.5(\text{major axis})(\text{minor axis})^2$ or the equation for the volume of an ellipsoid with all 3 dimensions obtained from the images. Tumor 1: MRI volume = 1.13 mm^3; $0.5bc^2$ = 0.64 mm^3; ellipsoid = 0.69 mm^3. Tumor 2: MRI volume = 2.09 mm^3; $0.5bc^2$ = 1.44 mm^3; ellipsoid = 1.67 mm^3.

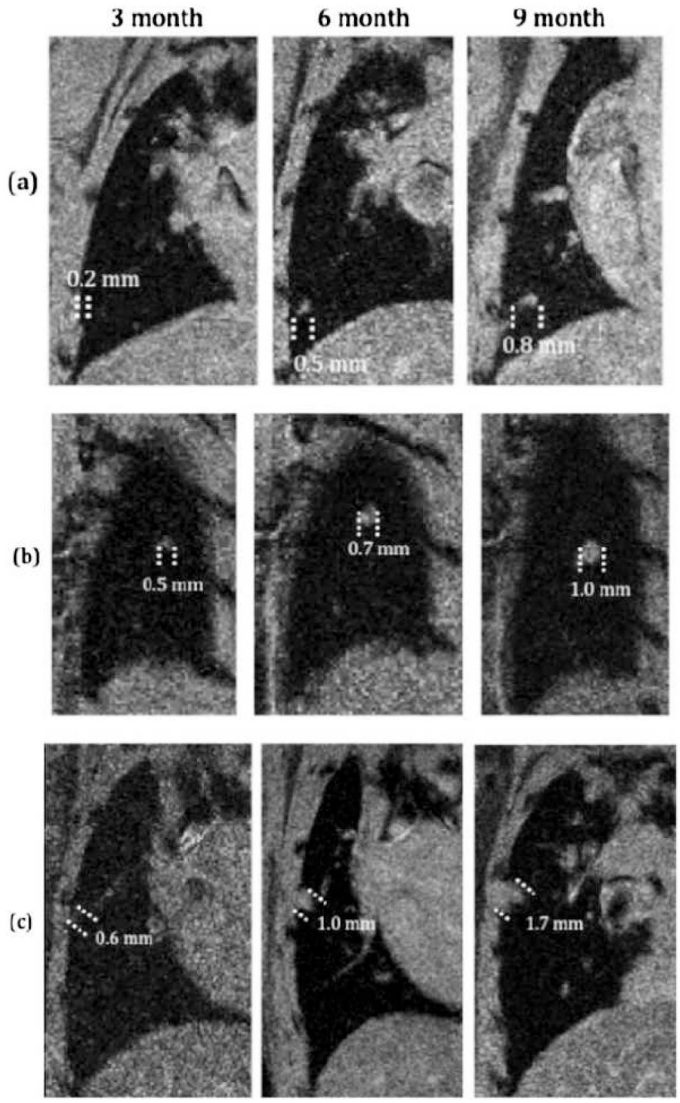

FIG. 3.
MR lung images from MC+BHT mice demonstrating the capability to longitudinally assess *in vivo* tumor growth: (a) unirradiated control; (b) irradiated with 4 fractions of 30 mGy; (c) irradiated with 4 fractions of 50 mGy.

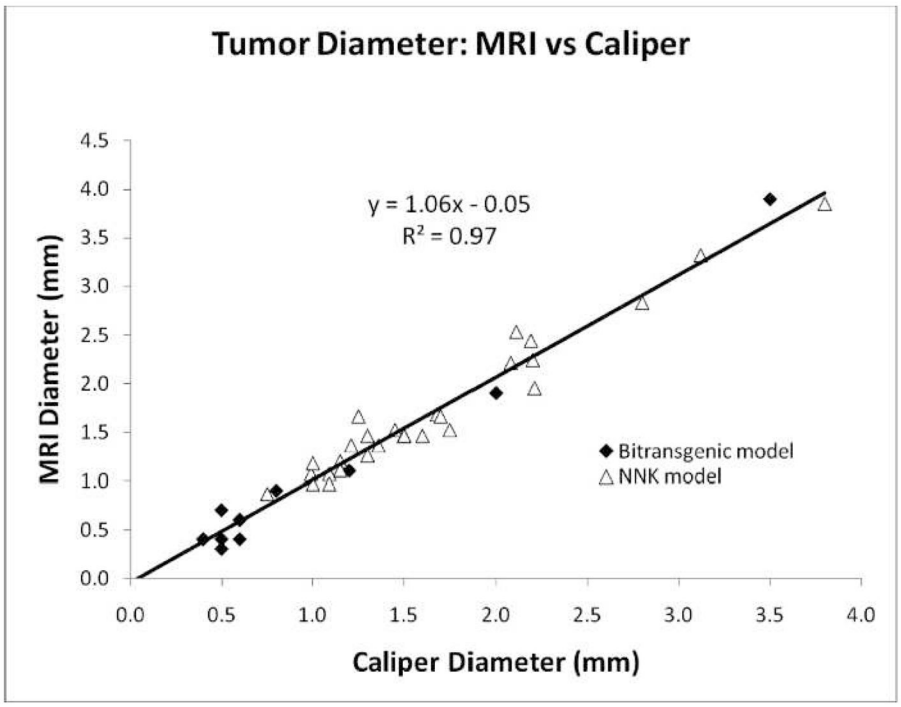

FIG. 4.

A comparison of lung tumor diameters at 9 months postirradiation measured *in vivo* using our double-gated 7T MRI technique and *ex vivo* using electronic calipers after excising the lungs. The data are for tumors from the bitransgenic (closed diamonds) and NNK (open triangles) mouse models.

TABLE 1

Tumor Size and Growth as a Function of Postirradiation Time and Dose

Radiation dose	3 month [mm^3]†	6 month [mm^3]†	9 month [mm^3]†	Growth rate* [ln(mm^3)/month]†	Growth curve R^2	Volume doubling time (months)
Sham (n = 14, 5)#	0.18 (0.05)	0.80 (0.16)	3.29 (1.07)	0.46 (0.04)	0.97	1.5
10 mGy × 4 (n = 8, 4)#	0.31 (0.07)	1.74 (0.57)	3.88 (1.15)	0.39 (0.07)	0.84	1.8
30 mGy × 4 (n = 14, 4)#	0.36 (0.21)	1.01 (0.37)	4.03 (1.83)	0.41 (0.05)	0.97	1.7
50 mGy × 4 (n = 14, 4)#	0.30 (0.10)	1.29 (0.44)	2.70 (0.70)	0.41 (0.05)	0.93	1.7

#Number of tumors, number of mice.

†Values in parentheses are standard errors of the means.

*The tumor growth rate was determined from a linear regression analysis of the $\log_e$ transform of the individual tumor sizes as a function of time after the last fraction of irradiation.